Li *et al. Carbon Research* (2025) 4:23
https://doi.org/10.1007/s44246-024-00185-2

Carbon Research

ORIGINAL ARTICLE

Open Access

Fly ash-doped biochar fabricated by pyrolysis and hydrothermal strategies: characteristics and potentialities of carbon sequestration

Gang Li[1†], Rongchuan Ye[2,3†], Shumin Wu[2,3], Xianghui Liu[4], Meijing Huang[3], Jianda Guo[2,3,5], Yan Gao[2], Wei Chen[2*] and Yan Ma[3*]

Abstract

The oxidation of biochar occurs due to both natural and human influences during the soil carbon sequestration process. Therefore, it is crucial to produce high-stability biochar to achieve carbon neutrality. Fly ash-doped biochar was obtained from fly ash and corn stalks by employing hydrothermal/pyrolysis treatment, along with alkali impregnation at different temperatures. The microstructural characteristics and carbon sequestration potentials were studied as an essential performance parameter that was influenced by mineral doping and treatment temperature. The yield and carbon retention of P500-1:2 improved by 54.15% and 6.81%, respectively, and the carbon loss following H_2O_2 oxidation was only 9.93% as depicted by the results. In comparison with hydrothermal biochar, pyrolysis biochar is superior in terms of its carbon sequestration potential. SiO_2, Al_2O_3 and other components in fly ash continue to dissolve at high temperatures and react with carbon in biochar, promoting the formation of aromatic carbon and generating a physical protective layer to prevent biochar from oxidation, hence improving the chemical and thermal stability of biochar. High temperature and mineral interaction also contribute to high aromatic structure (H:C < 0.4) formation, significantly improving the specific surface area and thermal stability of biochar.

Highlights

- Fly ash-doping is more effective in enhancing carbon retention and chemical oxidation resistance in pyrolysis biochar compared to hydrothermal biochar.
- Doping with fly ash improved the microstructure and promoted the aromatization of pyrolysis biochar, benefiting carbon retention.
- As the temperature increased, the carbon retention of fly ash-doped biochar gradually decreased, with the rate of change stabilizing.

[†]Gang Li and Rongchuan Ye contributed equally to this work.

*Correspondence:
Wei Chen
wchen@jaas.ac.cn
Yan Ma
mayan2202@163.com
Full list of author information is available at the end of the article

• The addition of fly ash facilitated the formation of Si-C/Al-C bonds, contributing to the chemical oxidation resistance of the biochar.

Keywords Biochar, Fly ash, Pyrolysis, Hydrothermal, Carbon sequestration

Graphical Abstract

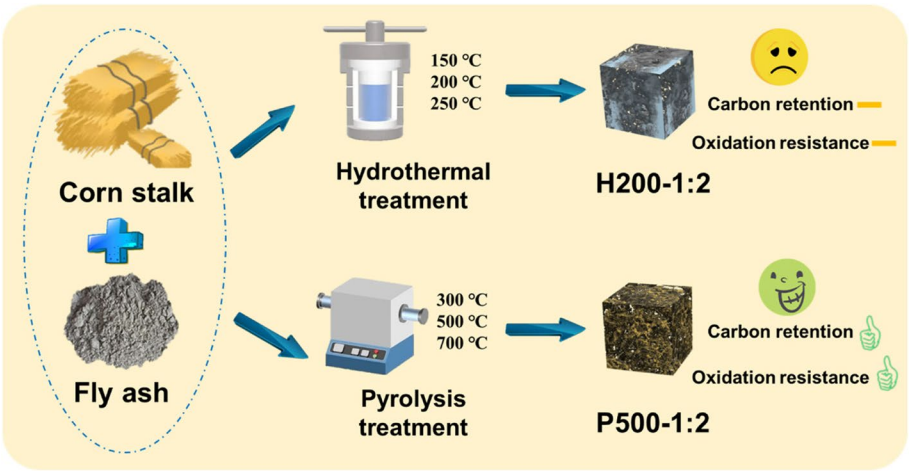

1 Introduction

Biochar can be produced under hypoxic conditions, using either hydrothermal or pyrolysis methods. The hydrothermal method typically occurs at temperatures between 180 ℃ and 250 ℃ under elevated pressure. In this process, water aids in the decomposition and polymerization of biomass, leading to biochar formation. Pyrolysis, on the other hand, involves heating biomass to high temperatures (usually between 300 ℃ and 700 ℃) in an oxygen-deprived environment. This breaks down its organic components, converting the biomass into biochar. Biochar has attracted scientific attention owing to its potential to improve soil properties, increase crop yield, and stabilize pollutants (Yang et al. 2022; Majumder et al. 2019; Zhou et al. 2021; Wu et al. 2024). Biochar has been suggested to mitigate climate change by sequestering carbon (Leng and Huang 2018; Kan et al. 2020; Shin et al. 2021; Wang et al. 2023). Accordingly, the cost of negative emissions for biochar from agricultural and forestry wastes is capped at < 100 \$ t^{-1} CO_2 in China. Although biochar from crops and grass is more expensive due to high biomass purchasing cost, they are still more economic than other techniques, such as CO_2 fuels (0–670 \$ t^{-1} CO_2), DACCS (30–1000 \$ t^{-1} CO_2), and microalgae (230–920 \$ t^{-1} CO_2) (Babin et al. 2021; Lane et al. 2021). Biochar application technology is both commercially feasible and economically favorable, suggesting that biochar could be regarded as a relatively cost-effective material for carbon sequestration (Deng et al. 2024). The properties of biochar, including carbon content and stability, are indispensable factors affecting the application of biochar in soil (Pereira et al. 2011; Johannes and Stephen 2012; Sun et al. 2020; Tomczyk et al. 2020; Chen et al. 2024). The stability of biochar is primarily influenced by its aromatic chains, surface functional groups and porous structure. These properties can be affected by the interaction between temperature and mineral doping during pyrolysis or hydrothermal treatment (Han et al. 2018; Zhao et al. 2019; Lu et al. 2020; Wang et al. 2022c). Hence, it is significant to devise strategies for regulating pyrolysis and hydrothermal carbonization to attain appropriate carbon retention and stability of biochar.

Minerals have a significant influence on biomass pyrolysis and hydrothermal processes, catalyzing the reaction and affecting the conversion of biomass, thereby improving biochar stability and resulting in a more porous structure (Akanksha et al. 2022). The addition of silica in the biomass pyrolysis and hydrothermal process reduced the H/C and O/C atomic ratio of biochar, which contributes to the chemical oxidation resistance and thermal tolerance (Zhao et al. 2019). Silicon participates in the formation of carbon structure by forming C-Si bonds, which improves the stability of biochar (Ahmad et al. 2019; Zhao et al. 2019; Wang et al. 2022a, b, c). Fly ash is a promising mineral additive due to its high silicon

content. The incorporation of mineral components in fly ash (e.g., Si and Al) and carbon from biomass promotes the porous structure and reducing the mineral crystal size, which contributes to the specific surface area and porosity of biochar. Fly ash itself may also form micropores or mesoporous structures in biochar, especially when the pyrolysis temperature is high, the structure of fly ash may be partially melted and resolidified to form new pores (Yun et al. 2022). In addition, alkali, as well as alkaline earth metals (K, Na, Ca, and Mg), have been shown to promote the cleavage of low molecular compounds in cellulose, and above certain levels of alkali metals, that can increase carbon yield (Williams and Horne 1994; Patwardhan et al. 2010). Modified biochar with NaOH, dehydration of NaOH during carbonization led the carbon skeleton to aromatize, prevented the destruction of biochar structure and promoted the reduction of carbon, which in turn caused the aromatic ring structure and aromatic structure in the adsorbent to undergo (π-π) conjugation with each other (Liu et al. 2020a; Wang et al. 2022a). The use of sodium hydroxide alkali fusion fly ash in biomass pyrolysis to produce biochar was previously investigated by our group and it was found that the yield, porosity, and specific surface area of biochar were considerably improved by the method (Yun et al. 2022). In our previous work, fly ash-doped biochar was successfully synthesized for Pb remediation (Ma et al. 2024). However, further investigation is needed to understand the effects of pyrolysis/hydrothermal processes, mineral doping and alkali dipping on the properties of biochar.

The stability and carbon retention of biochar are strongly correlated with the fabrication temperature, which is a critical element influencing the characteristics of biochar. Most research indicates that high-temperature biochar includes a greater amount of aromatic carbon, which is more stable and difficult to biodegrade chemically, whereas low-temperature biochar contains more aliphatic carbon, which is more volatile and can be chemically broken down rather conveniently (Liu et al. 2020a; Wang et al. 2021a, b; Zong et al. 2020). A kind of biochar co-pyrolyzed by wood and bentonite/kaolin under 350 °C, 450 °C, and 550 °C was reported. According to the results, the carbon loss of the materials synthesized at 550 °C after hydrogen peroxide oxidation was decreased to no more than 19.2%, and the deposition index (R_{50}) of biochar was enhanced to no less than 0.89, 4.89 mg g^{-1} of dissolved organic carbon remained after reduction (Wang et al. 2022b). To produce biochar within a temperature range of 300 to 800 °C, the biochar yield and polarity exhibited a decreasing trend when the pyrolysis temperature was elevated (Fan et al. 2022). High pyrolysis temperature (> 500 °C) reduced the biochar yield, but increased the aromatic structure, pH value, pore size, and the number of C–C bonds, whereas the number of C-O and O–H bonds was found to decrease (Aktar et al. 2022; Ahmad et al. 2019).

Various studies have been conducted to investigate the impact of minerals and fabrication temperature on the carbon conversion process. The primary emphasis of these studies lies in examining the impact on the generation of reaction intermediates and the physicochemical characteristics of resulting products. Nevertheless, the current body of research on the impact of fabrication conditions and mineral interaction on carbon sequestration is quite scarce (Yang et al. 2018). However, there is only a limited volume of research examining the influence of temperature and mineral doping on the characteristics of biochar, specifically in relation to its carbon structure and resistance to oxidation. In this study, corn stover biomass and fly ash, mixed with alkali impregnation were pyrolyzed and hydrothermally treated slowly at 300 °C, 500 °C, 700 °C and 150 °C, 200 °C, 250 °C to produce biochar. Synchronous thermal analyzer (TG-DSC), X-ray photoelectron spectroscopy (XPS), Fourier transform infrared spectroscopy (FTIR), and additional techniques were employed for the characterization of biochar. The manipulation of fabrication temperature and the introduction of mineral additives during the production process resulted in alterations to the physicochemical characteristics of biochar, thereby influencing its stability. The primary objectives of this work may be outlined as follows: (1) to investigate the impact of fabrication temperature and the addition of fly ash on the microstructural characteristics of biochar; (2) to examine the impact of fly ash doping on the stability of biochar and explore potential strategies for enhancing stability; (3) compare the biochar synthesized through pyrolysis and hydrothermal treatment and valuate their carbon sequestration potential.

2 Materials and methods

2.1 Materials

Fly ash (FA) was collected from a coal-fired power plant in Shanxi Province, China. The fly ash sample was dried in an oven at 85 °C, screened through an 18-mesh sieve, and stored in a ziplock bag at room temperature for later use. Corn stover (CS) was planted under soil cover in a coal gangue dump in Changzhi, Shanxi Province, air-dried, crushed through an 18-mesh sieve, and dried in an oven (85 °C).

2.2 Biochar production

The pyrolysis process has been described briefly below. Initially, a mixture of FA and CS was prepared with 50% w/w and 20% w/w, respectively. A 5 mol L^{-1} NaOH solution was added to the mixture, with a solid–liquid ratio

of 1:10. The resulting mixture was subjected to oscillation at a speed of 150 r min^{-1} for 8 h, following which the mixture was filtered, dried and ball-milled for further process. Subsequently, CS and two mixes were introduced into a tube furnace under a continuous flow of nitrogen gas. The furnace was heated at a rate of 10 °C min^{-1} until predetermined temperatures of 300, 500, and 700 °C were reached and sustained for 2 h. The samples were subjected to a thorough cleaning process involving multiple rinses with deionized water until the pH value reached a steady state. The corn stover biochar obtained by the pyrolysis method was named P500-BC, and alkali-impregnated fly ash biochar were named P500-1:2, P500-1:5, P300-1:2, and P700-1:2, respectively.

The hydrothermal process was conducted as follows. First, Fly Ash (FA) and Corn stalk (CS) were mixed in ratios of 0:1, 1:2 and 1:5. This mixture was then combined with 5 mol L^{-1} NaOH solution at a ratio of 1:10. The resulting mixture was stirred at 150 rpm for 8 h to ensure thorough mixing of FA mineral components and CS. Next, the mixture was placed in a steel reactor for hydrothermal treatment at temperatures of 150 °C, 200 °C and 250 °C, respectively. After the hydrothermal reaction, the slurry was cooled to room temperature, then filtered and washed with deionized water more than 3 times until the pH stabilized. Finally, the alkaline hydrothermal FA-doped biochar was obtained by drying at 105 °C in an oven for 12 h. The corn stover biochar obtained by the hydrothermal method was named H200-BC, and alkali-impregnated fly ash biochar were named H200-1:2, H200-1:5, H150-1:2, and H250-1:2, respectively (Table 1).

2.3 Biochar characterization

Biochar yield at different temperatures was estimated according to the dry weight ratio of biochar to raw material. The retention of carbon in the biochar following pyrolysis was computed according to the carbon content and yield.

$$\text{Yield } (\%) = (W_1/W_2) \times 100\% \quad (1)$$

$$\text{Carbon retention } (\%) = [(C_1 \times \text{Yield})/(aC_2 + bC_3)] \times 100\% \quad (2)$$

where W_1 and W_2 are the dry weights (g) of biochar and its feedstock. C_1 is the carbon content of biochar. C_2 and C_3 represent carbon contents of biomass and fly ash, and a, b are the mass ratio of biomass and fly ash, respectively.

Measurement of pH value was made in a deionized aqueous solution with a mixture ratio of 1:20 (w/v) and 180 r min^{-1} oscillation. After 24 h of equilibrium, the pH of the supernatant is recorded using a pH meter (FE28-Standard, Switzerland). The ash content was determined by heating at 815 ± 10 °C for 1 h. Elemental analyzer (Elementar UNICUBE, Germany) was used to analyze the amount of C, H, N, and S in all specimens. The results of the above indicators have been summarized in Table S1.

The microstructural details of the specimens were observed by scanning electron microscopy and an energy spectrum analyzer (Hitachi Regulus 8100, Germany), The powder samples' specific surface area and pore size distribution were ascertained by utilizing a BET-N_2 SA analyzer (ASAP 2460 microcrystallography (USA)). Using an X-ray diffractometer (Ultima IV, Japan) with a scanning range of 5–80° and a scanning speed of 2° min^{-1}, the sample's crystal structure was examined. MDI Jade was used to assess the scanning results. Using Fourier transform infrared spectroscopy (Nicolet iS 10, USA), the surface functional groups of biochar were observed in the 4000–400 cm^{-1} range and distinguished by FT-IR Spectral Library. X-ray photoelectron spectrometer (Thermo Fisher ESCALAB, USA) was utilized to examine the sample's valence state and molecular structures. The peaks fitting was achieved by using Thermo Scientific Avantage 6.6.0.

Table 1 Abbreviation and information

Abbreviation	Fly ash/ biomass ratio (g/g)	Temperate (℃)	Method
H200-BC	0:1	200	Thermal hydrolysis
H200-1:2	1:2	200	
H200-1:5	1:5	200	
H150-1:2	1:2	150	
H250-1:2	1:2	250	
P500-BC	0:1	500	Pyrolysis
P500-1:2	1:2	500	
P500-1:5	1:5	500	
P300-1:2	1:2	300	
P700-1:2	1:2	700	

2.4 Analysis of antioxidant activity

The oxidation resistance of all biochar samples was studied to assess the stability of biochar, using two methods (chemical oxidation and TGA).

Thermogravimetric curves of biochar were obtained using TG-DSC (TA, USA). The analysis method is as follows. The sample was ground to be measured evenly. The sample (5 mg) was placed in the crucible, and put into the analysis chamber for analysis. The sample was subjected to thermal analysis in the temperature range of 30 °C to 900 °C, the heating rate was 20 °C min^{-1}, the carrier gas was N_2, and the gas flow rate was 100 mL min^{-1}.

The ratio of volatile organic-C (degradation range of 30–200 ℃), labile organic-C (cellulose, aliphatic-C, and

carbohydrates with a degradation range of 200–380 ℃), recalcitrant organic-C (lignin and aromatic C with a degradation range of 380–475 ℃), refractory organic-C (poly-condensed forms of lipids and aromatic-C with a degradation range of 475–600 ℃), and inorganic-C (elemental-C and carbonate with a degradation range of 600–1000 ℃) were calculated by the weight loss during TG analysis in their specific temperature sections (T1–T2) Eq. (3).

$$C_{loss}=\frac{C_{T1}-C_{T2}}{C_{total}} \tag{3}$$

Using H_2O_2 reagent, a chemical oxidation analysis was performed. H_2O_2 (5%, 35mL) was combined with 0.5 g of biochar in a 50 mL test tube and gently swirled for a minute. The test tube was covered and left to sit in a water bath set at a constant 60 °C for 48 h. After the heating procedure was complete, the test tubes were placed in a drying oven set at 105 °C for 60 h, or until the biochar reaches a consistent weight and the H_2O_2 evaporates. Equation (4) illustrates how the total carbon before and following H_2O_2 oxidation is used to calculate the quantity of carbon lost.

$$C_{loss}=\frac{C_1\times M_1-C_2\times M_2}{C_1\times M_1}\times 100\% \tag{4}$$

Among them, C loss represents the carbon loss after 5% H_2O_2 oxidation of biochar, %; C_1 and C_2 represent the carbon content of biochar before and after oxidation, respectively, %; M_1 and M_2 respectively represent the mass of biochar before and after oxidation, g. The aromaticity index (AI) of biochar was also calculated based on Eq. (5).

$$AI=\frac{1+[C]-[O]-0.5[H]}{[C]-[O]-[N]} \tag{5}$$

2.5 Statistical analysis

In this study, Microsoft Excel 2019 was used to statistically process the experimental data, Origin 9.5 software was used to map the processed data, and Jade 6.0 software was used to analyze the XRD patterns. The correlation and significance were analyzed by SPSS software.

3 Results and discussion

3.1 Effect of fly ash doping on basic physicochemical properties of biochar

In terms of yield, elemental content, pH, and other factors, Table S1 compares and summarizes the physical and chemical properties of ten different types of biochar. The carbon content in both original biochar (P500-BC and H200-BC) is higher than that in corn straw biomass, indicating that converting straw biomass into biochar is beneficial for carbon sequestration. The organic element content in the original biochar is generally higher than that have fly ash added. This difference is attributed to the increased ash content from doped fly ash. During the carbonization process, biochar releases functional groups containing hydrogen and oxygen, while carbon is volatilized as gas and liquid, leading to a significant reduction in the organic elements of C, H, O and N. It is important to note that the preparation temperature influences the carbon content of the biochar. As the temperature increases, the heating process intensifies, resulting in a decrease in carbon content (Liu et al. 2021).

Compared to the initial biochar, the yield increased with the addition of fly ash, which is influenced by the thermal stability of the raw materials. However, this trend does not apply to H200-1:5, likely due to the low proportion of fly ash, which is crucial for the formation of hydrothermal carbon. This low proportion results in increased gas and liquid production in hydrothermal products, leading to a decrease in yield. Regarding preparation temperature, the yield is negatively correlated with hydrothermal temperature. However, when the temperature exceeds 200 ℃, the yield shows no significant changes with the same feedstock and conditions, indicating that the mass of biochar does not significantly decrease beyond this temperature.

The breakdown of organic components in biochar during pyrolysis at elevated temperatures is the primary cause of the loss in biochar output and increase in ash content that results from raising the pyrolysis temperature (Ren et al. 2018; Wang et al. 2022b). As can be seen from Table S1, while the pyrolysis temperature increased from 300 °C to 700 °C, the biochar yield of 50% fly ash doping decreased from 92.14% to 78.05%. The yield of biochar increased with the higher fly ash doping ratio, and the yield of P500-BC was only 29.10%, while the yield of P500-1:2 and P500-1:5 increased to 83.25% and 79.59%, respectively. It shows that fly ash has a high resistance to thermal degradation (Ahmad et al. 2019; Zhao et al. 2019). According to the findings of the elemental analysis, the mass ratio of the elements C, H, O, and N in AB dramatically dropped. Fly ash increases the number of inorganic components in biochar, which decreases the proportion of organic components; however, during pyrolysis, biochar releases functional groups containing hydrogen and oxygen, greatly reducing the amounts of hydrogen and oxygen elements (Wang et al. 2020b). All pyrolysis biochar were alkaline, the addition of fly ash resulted in a higher pH value. The alkalinity of the biochar tends to grow as the amount of fly ash used for doping increases because the alkaline oxides in the fly ash promote a rise in the biochar's alkalinity (Bhardwaj

et al. 2022). As the preparation temperature increases, the alkalinity of biochar also increases. When the preparation temperature is 700 °C, the pH value of biochar reaches 11.53, which is due to the formation of alkaline functional groups under high-temperature conditions.

3.2 Oxidation resistance of biochar

Figures 1a, b and S1a, b show the thermogravimetric and derivative thermogravimetric curves of biochar. Based on the TG analysis, carbon loss can be attributed to different species during various temperature intervals (Fig. 1c, d): volatile organic-C, labile organic-C, recalcitrant organic-C, refractory organic-C and inorganic-C (Xu et al. 2021). The TG curves of hydrothermal biochar with different temperatures and fly ash doping ratios are different. The mass loss of the H200-BC is obvious with the increase in temperature because fly ash is not added. The H200-BC mainly goes through three stages: the first stage is from initial temperature to 300 ℃, which represents the dehydration of biochar. The mass loss depends on the water content of biochar, and its mass decreases slightly, about 7%–8% of the original mass. The second stage is 300 ℃ to 500 ℃, and the mass of hydrothermal biochar in this stage decreases rapidly, about half of the original mass is reduced, mainly because of the thermal degradation of hemicellulose in biomass. Then the decomposition of cellulose and the volatilization of products occurred. The last stage is 500 ℃ to 900 ℃, the mass loss rate at this stage is low, and the TG curve is stable. The mass loss at this stage is caused by the volatilization of lignin decomposed products at higher temperatures. However, except that the TG curves of the H150-1:2 and the H200-BC show a rapid downward trend, the other TG curves are similar and smoother, while the mass loss is significantly reduced. The reason is that the addition of fly ash increases the aromatic species of biochar and improves thermal stability. The hydrothermal carbon prepared at low temperature (150 ℃) contains more aliphatic carbon, leading to more mass loss compared with other hydrothermal biochar, which is consistent with the analysis results of the Van-Krevelen diagram (Bhardwaj et al. 2022).

Pyrolysis biochar has a certain mass loss in the process of temperature rise. Pyrolysis biochar is quite stable thermally as inferred by its mild mass loss (25% of initial biochar) when the temperature reached 900 °C. The stability of biochar is influenced to some extent by the temperature of pyrolysis. The thermal stability of biochar improved as the temperature increased, due to the formation of aromatic carbon, regardless of whether the fly ash doping ratio remained constant (Liu et al. 2020b; Wang et al. 2020a; Zong et al. 2020). Furthermore, it is obvious that when subjected to the same pyrolysis temperature, the thermogravimetric curves of biochar produced with varying fly ash doping ratios demonstrate a high degree of similarity, except for the P500-1:5 sample. The derivative thermogravimetric curve indicates that P500-1:5 exhibits a significant reduction in mass above 500 °C. This phenomenon can be attributed to the substantial presence of straw biomass in the composition of sample P500-1:5, leading to the thermal degradation of hemicellulose and cellulose present in the biomass (Dumanlı and Windle 2012). A few studies have reported the use of chemical oxidants, for instance, potassium dichromate, potassium permanganate, nitric acid, and hydrogen peroxide, to evaluate the oxidation resistant properties of biochar and determine its long-term stability (Ahmad et al. 2019; Ren et al. 2018; Yang et al. 2018). A comparison of the TG curves between hydrothermal and pyrolysis biochar, revealed that of biochar produced through pyrolysis had less mass loss. This is likely due to the lower temperature range used in the hydrothermal method (150–250 ℃). The higher temperatures of pyrolysis method (300–700 ℃) resulted in the formation of more stable aromatic carbon. This finding aligns with the results of H/C and O/C atomic ratio analysis.

The carbon loss rate of hydrothermal biochar after H_2O_2 oxidation is shown in Fig. 1e. As the temperature rises from 150 ℃ to 250 ℃, the carbon loss rate increases from 9.23% to 24.65% (H150-1:2, H200-1:2, H250-1:2). This indicates greater carbon loss and reduced chemical stability at higher hydrothermal temperatures. The increased carbon loss is likely due to the higher reaction rate between hydroxyl radicals and amorphous aromatic carbon at elevated temperatures (Werner and Yao 1992; Li et al. 2015). At higher hydrothermal temperatures, more amorphous aromatic carbon is generated compared to biochar produced at lower temperatures, making low-temperature hydrothermal biochar more chemically stable. As hydrothermal temperature increases, the reaction of carbon-containing organic matter in the biomass intensifies, leading to higher production of soluble substances and gases, which in turn causes greater carbon loss in the biochar. Under the same hydrothermal conditions, H200-BC showed the highest carbon loss rate of 16.21%, which gradually decreased as the proportion of fly ash increased. This suggests that adding fly ash helps protect biochar from H_2O_2 oxidation and improves its chemical stability.

For pyrolysis biochar, the P700-1:2 had a carbon loss rate of merely 8.56%. Moreover, it was observed that the carbon loss rate of biochar exhibited a notable reduction as the temperature increased, while maintaining a constant ratio of fly ash addition (Fig. 1f). Nevertheless, it is important to note that the carbon loss rate of P500-1:2 is 9.93%, albeit slightly lower than that of P700-1:2.

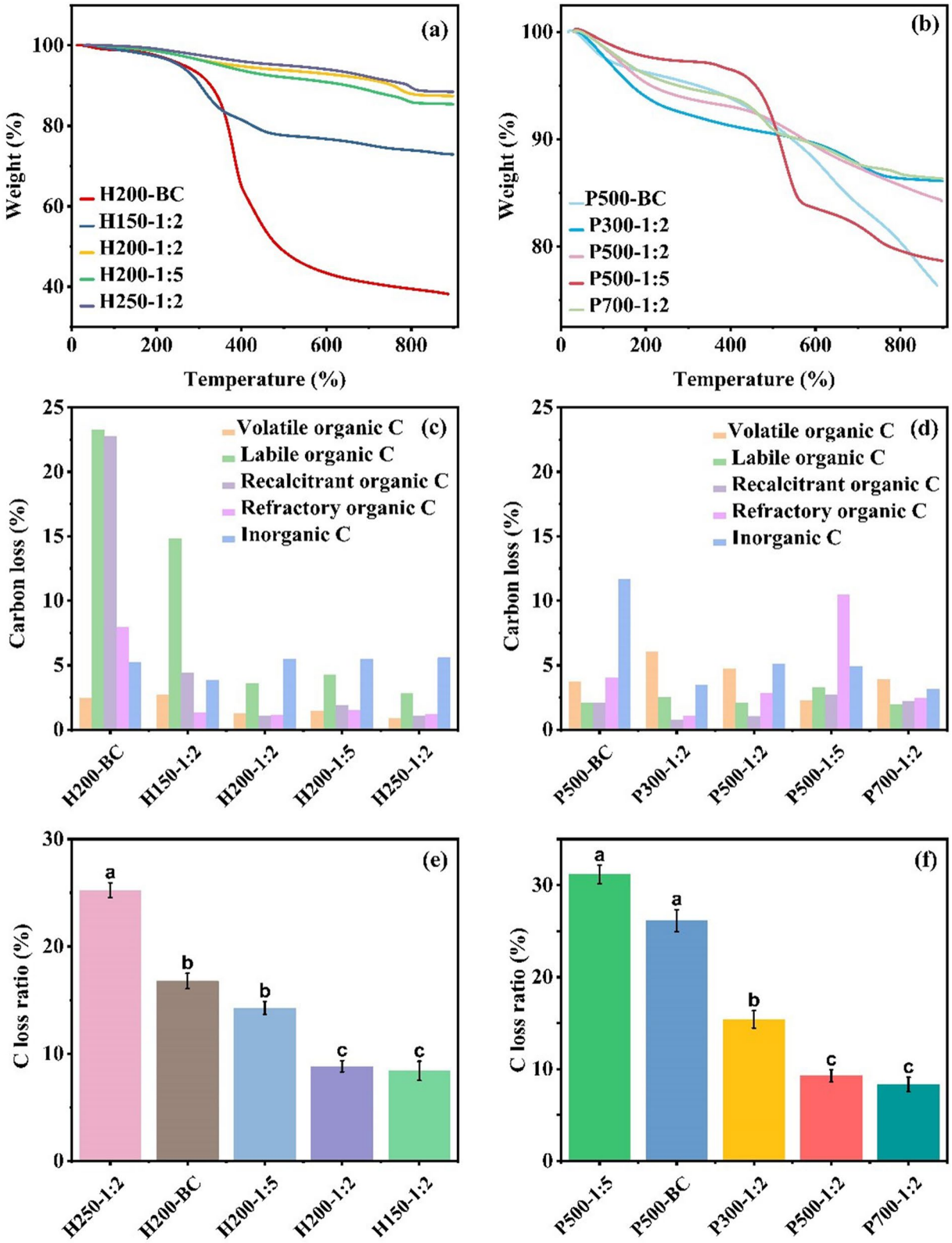

Fig. 1 TG curve of hydrothermal biochar (**a**) and pyrolysis biochar (**b**); Carbon loss proportion of hydrothermal biochar (**c**) and pyrolysis biochar (**d**) obtained by TG analysis; Carbon loss rate of hydrothermal biochar (**e**) and pyrolysis biochar (**f**) during 5% H_2O_2 oxidation process

However, there is no significant difference between P500-1:2 and P700-1:2 ($p > 0.05$), it can be concluded that the biochar produced at a temperature of 500 °C exhibits robust chemical oxidation resistance and offers certain energy conservation. Furthermore, it can be deduced that the carbon loss rate of biochar exhibits a reduction when the fly ash doping ratio increases. This finding suggests that fly ash has an indispensable role in enhancing the chemical stability of biochar (Wang et al. 2020a, 2021b). P500-1:5 and P500-BC are similar, possibly attributed to the addition of a small amount of fly ash which was mainly used as a catalyst to promote the hydrolysis of biomass, leading to the collapse of pore structure. Finally, biochar characterization verified the decline in carbon retention rate and chemical stability.

3.3 Biochar structure and its relationship to carbon retention and stability

The SEM images of fly ash-doped hydrothermal biochar are shown in Fig. 2a-d. Biochar without fly ash exhibits a dense spherical porous structure, formed by hydrothermal process (Fig. S2a). After doping with fly ash, the pore structure on the biochar surface expanded, and the fly ash transformed into octahedral zeolite following alkali impregnation and hydrothermal treatment, consistent with the XRD analysis (Fig. 4d). The zeolite generated adheres to both the surface and internal structure of biochar, improving its pore structure. The fly ash coating helps reduce biochar oxidation. The hydrothermal temperature significantly impacts biochar structure, with the zeolite expanding as the temperature increasing. At 150 ℃, the surface pores of hydrothermal carbon structure are blocked, likely due to incomplete reactions and limited microstructural changes. EDS mapping (Fig. S3a-e), was used to evaluate the elemental composition of biochar surfaces. Biochar without fly ash had the highest carbon content, which decreased significantly after fly ash doping. Sodium was also detected on the biochar surface, a result of the NaOH impregnation process.

P500-BC (Fig. S2b) demonstrates a smooth surface, porous structure and flat channel, while pyrolysis FA-doped biochar demonstrates a rough surface with obvious folds, and collapsed pores (Fig. 2e-h). In accordance with Table S1 and Fig. S3, the biochar structure gradually transformed along with the temperature from a dense but small porous structure (P300-1:2) to one with clearly large pores (P700-1:2). However, the specific surface area and total pore volume decreased. It is hypothesized that under pyrolysis conditions, components like SiO_2 and Al_2O_3 in fly ash react with carbon in biochar, causing the carbon layer to collapse and sag and altering the surface microstructure of carbon (Wang et al. 2020a). Simultaneously, the mineral composition of fly ash envelops the surface of biochar, facilitating the generation of a physical protective layer around the biochar. This layer serves to diminish and impede the impact of external environmental variations on the biochar, thereby restraining the decomposition and subsequent emission of carbon molecules (Wang et al. 2022b). It is found in Fig. S3 that the C content of P500-BC and P500-1:5 is high, while the inorganic components of the rest biochar account for a large proportion, indicating that the doped fly ash adheres to the surface of biochar or enters the pores of biochar.

The specific surface area, average pore size and pore volume characteristics of biochar prepared by the hydrothermal method are shown in Table S1, the N_2 adsorption/desorption curve and pore size distribution of hydrothermal biochar are demonstrated in Fig. 3a, b.

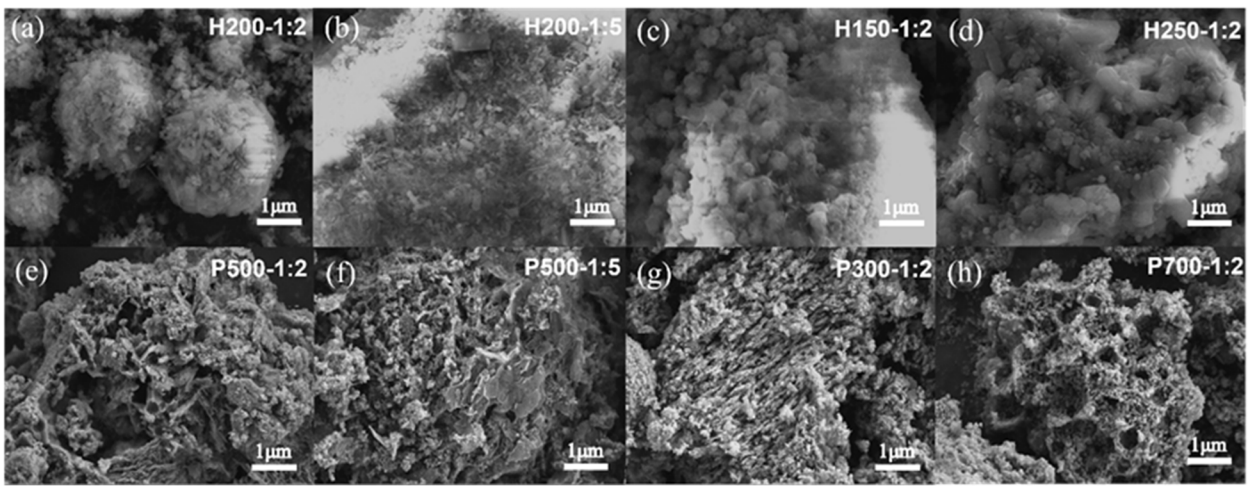

Fig. 2 The scanning electron microscope (SEM) images of fly ash doped hydrothermal biochar (**a**, **b**, **c**, **d**) and pyrolysis biochar (**e**, **f**, **g**, **h**)

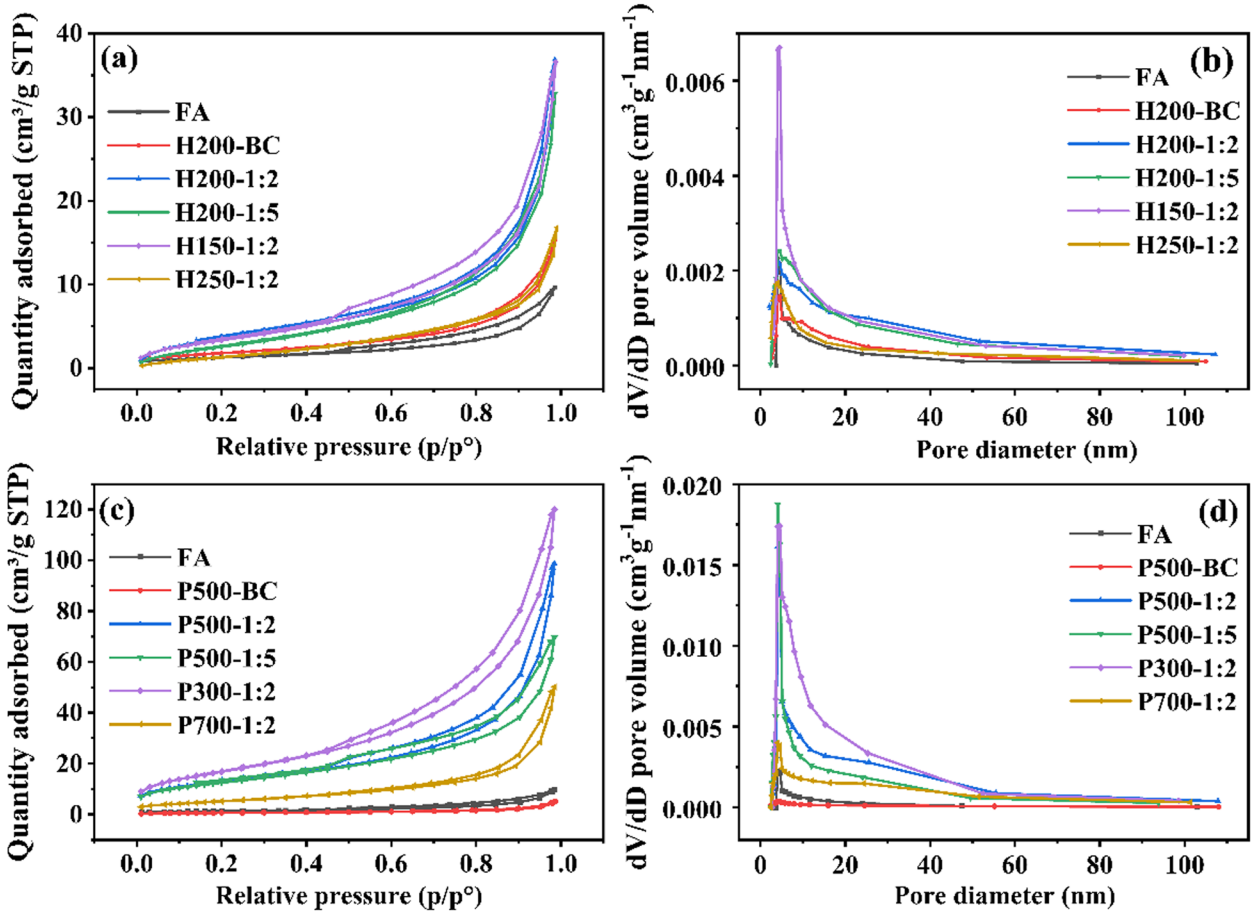

Fig. 3 N_2 adsorption and desorption curve of hydrothermal biochar (**a**) and pyrolysis biochar (**c**); pore size distribution of hydrothermal biochar (**b**) and pyrolysis biochar (**d**)

Overall, the specific surface area (SSA), average pore diameter (APD) and pore volume (PV) of hydrothermal biochar did not change significantly. Different hydrothermal temperatures and fly ash doping ratios had a limited effect on the SSA of biochar. When the hydrothermal temperature was constant, the SSA of biochar slightly increased with higher fly ash addition, though the improvement in pore characteristics was minimal. Fly ash may have a catalytic activation effect during the hydrothermal process, leading to an increase in the biochar's specific surface area. However, excessive fly ash addition can cause pore blockage. The SSA and pore volume of biochar are significantly influenced by hydrothermal temperature. It can be seen from Fig. 3a that when the preparation temperature reaches 250 ℃, the N_2 adsorption capacity of the biochar decreases significantly. This indicates a reduction in the SSA and PV of the hydrothermal biochar under these conditions, with values dropping to just 6.04 m^2/g and 0.03 cm^3/g, respectively. The likely reason for this decline is that the high hydrothermal temperature causes pore blockage in the biochar (Wang et al. 2019).

The SSA and PV of pyrolysis biochar were both enhanced by fly ash doping during pyrolysis treatment. P500-1:2 exhibited an eight-fold increase in specific surface area and a nine-fold increase in pore volume compared to P500-BC (Table S1). In contrast, biochar synthesized by hydrothermal method did not exhibit similar changes after fly ash doping. This can be attributed to the catalytic effect of fly ash doping in the pyrolysis process, which promotes the opening and expansion of micropores, resulting in a significant increase in PV and SSA. Interestingly, although the APD increased, the SSA and total PV of biochar decreased as the pyrolysis temperature rose. This contradicts most reported findings, and a possible explanation is that at higher temperatures, the pore size expands, leading to the collapse of pores and carbon layers (Rawal et al. 2016). The N_2 adsorption and desorption curve of biochar shows a BET type IV isotherm with an H_3 type hysteresis loop, indicating that

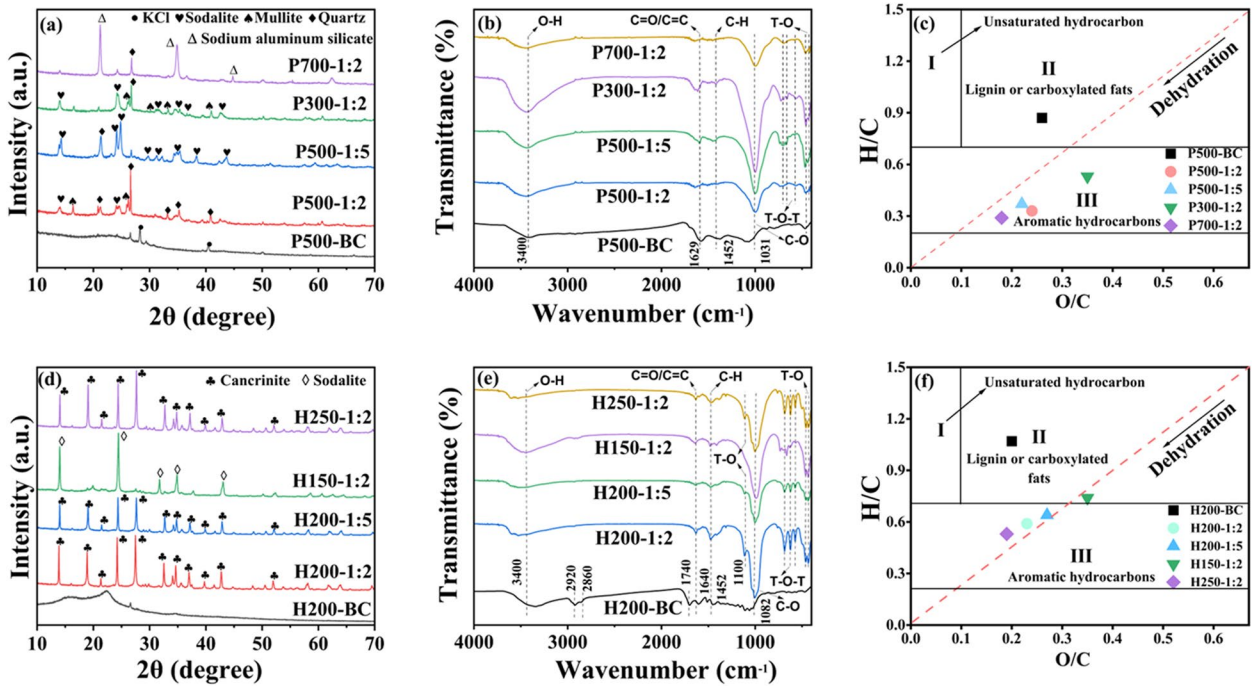

Fig. 4 X-ray diffraction patterns of pyrolysis biochar (**a**) and hydrothermal biochar (**d**); Fourier transform infrared spectroscopy of pyrolysis biochar (**b**) and hydrothermal biochar (**e**); Van-Krevelen diagram of pyrolysis biochar (**c**) and hydrothermal biochar (**f**)

the biochar consists of flaky particles or porous materials (Fig. 3c). The pore size of biochar ranges from 2 to 50 nm and is mainly composed of mesopores (Fig. 3d). The pore size distribution of P500-BC is narrow and significantly lower than that of fly ash-doped biochar. This indicates that fly ash plays a specific catalytic role during the pyrolysis process, enhancing the specific surface area and pore volume of biochar, as supported by several published studies (Wang et al. 2020a; Bhardwaj et al. 2022).

As the temperature increases, the carbon retention of biochar gradually decreases with the rate of decrease becoming less pronounced at higher temperatures. With a fly ash doping ratio of 1:2, the carbon retention values for biochar are as follows: 55.03% (P300-1:2), 45.50% (P500-1:2), 37.80% (P700-1:2) and 24.84% (H150-1:2), 15.81% (H200-1:2), 15.49% (H250-1:2) (Table S1). This may be caused by the breakdown of alkyl groups in biochar with increasing temperature (Fig. 4b), indicating that the degree of aromatization of biochar continues to improve. In addition, the incorporation of fly ash significantly enhanced the carbon retention of biochar, increasing from 29.1% (P500-BC) to 83.25% (P500-1:2) and from 30.72% (H200-BC) to 36.7% (H200-1:2) (Table S1). During the subsequent hydrothermal and pyrolysis stages, fly ash helps minimized the release of C, H, and O as small molecules, accelerates the dehydration of biomass, and limits the formation of L-glucan. These combined effects result in improved yield and carbon retention (Dumanlı and Windle 2012). Similar findings have been consistently reported in many previous studies (Li et al. 2014; Ren et al. 2018; Wang et al. 2022b). Thus, the most effective for producing biochar from raw materials, as demonstrated in our previous studies, is NaOH-treated fly ash, which achieves a high yield and carbon retention rate, making it beneficial for carbon sequestration.

Compared with P500-BC, fly ash doped biochar contains crystalline quartz (SiO_2), mullite ($3Al_2O_3{\cdot}2SiO_2$) and other components (Fig. 4a; Sahoo et al. 2013). It indicates that fly ash is successfully loaded on biochar. It is worth noting that the components of SiO_2 and Al_2O_3 in fly ash continue to dissolve as the temperature rises, only albite is generated at 300 °C and 500 °C, and sodium silica-luminate is generated at 700 °C. Furthermore, the peak of the biochar prepared at 700 °C is higher than the peaks of the biochar prepared at 300 °C and 500 °C, suggesting that high temperatures boost the degree of crystallization of the biochar. Regarding hydrothermal biochar (Fig. 4c), the absence of a diffraction peak in H200-BC indicates a lack of crystal formation, suggesting that the composition is primarily amorphous. This finding implies that hydrothermal treatment may dissolve and leach inorganic components from the biochar (Fu et al. 2019). When comparing H200-1:2 and H200-1:5, it is evident that a higher proportion of fly ash leads to

stronger diffraction peak. To examine the impact of temperature (150 ℃, 200 ℃ and 250 ℃) during hydrothermal treatment, different mineral fractions (i.e., sodalite and cancrinite) were detected. This indicates that higher temperatures can disrupt the structure of fly ash and alter the structure and composition of biochar. The crystal structure becomes more pronounced as the temperature rising, as reflected by stronger diffraction peaks.

Figure 4b shows the absorption peaks of pyrolysis biochar appearing in FTIR spectra between 4000 cm^{-1} and 500 cm^{-1}. The peaks correspond to -OH (3400 cm^{-1}), C-H (1452 cm^{-1}), C=O/C=C (1629 cm^{-1}), C-O (1031 cm^{-1}), and T-O-T/T-O (500–800 cm^{-1}, where T represents Si or Al) (Nan et al. 2019). The presence of T-O and T-O-T indicates that the successful loading of SiO_2 and Al_2O_3 on biochar is consistent with the results of XRD observation. The stretching vibration of C-H, such as P700-1:2 and P500-1:2, weakens or even vanishes as the temperature and fly ash doping ratio rise, suggesting that the addition of fly ash and rising temperatures can encourage the transformation and breakdown of aliphatic carbon (Wang et al. 2014). Although the peaks at C=C/C=O (1629 cm^{-1}) and C-O (1031 cm^{-1}) underwent an indistinctive change in intensity after fly ash addition, the enhancement of aromatic carbon could be verified by the fine spectrum of C (Table S4), indicating that fly ash might promote the formation of biochar aromatic carbon, which is conducive to improving the stability of biochar (Yang et al. 2018; Awad et al. 2018; Xiao et al. 2018). The absorption peaks of hydrothermal biochar are quite similar to pyrolysis biochar (Fig. 4e), contain stretching vibration peak of O–H (3400 cm^{-1}), vibration peaks of T-O and O-T-O (near 1100 cm^{-1} and from 500 to 800 cm^{-1}), stretching vibration of C-H (1452 cm^{-1}), and the stretching vibration of C=C/C=O (1640 cm^{-1}). Biochar without fly ash-doping exhibits weak absorption bands at 2860 and 2920 cm^{-1}, corresponding to aliphatic C-H and asymmetric C-H stretching vibration, respectively. This suggests that the addition of fly ash reduces the amount of aliphatic carbon and enhances the stability. The stretching vibration of carboxylic acid functional groups appears at 1740 cm^{-1} (Bhardwaj et al. 2022). Following the addition of fly ash, the stretching vibration of carboxylic acid functional groups in the biochar disappeared, which can explain the pH value of the hydrothermal biochar changed from acidic to alkaline after fly ash doping. This change is beneficial as it helps reduce the degradation and volatilization of hydrothermal biochar.

One of the most important metrics indicating the stability of biochar is the H/C and O/C atomic ratio, which can reveal the degree of aromaticity and hydrophobicity in the material (Leng and Huang 2018; Liu et al. 2020a; Wang et al. 2022b; Yang et al. 2016). A lower H:C ratio indicates higher biochar stability as well as higher aromatization and carbonization (Chen et al. 2008; Oleszczuk et al. 2016; Xiao et al. 2016). Figure 4c shows that AB is in the position of aromatic hydrocarbons and BC is in the position of lignin or carboxyl-containing fats. This suggests that adding fly ash to biochar can convert the aliphatic groups into aromatic compounds and increase the stability of pyrolytic carbon, which is accord with the findings of XPS and infrared spectroscopy (Fig. 4b; Table S3). The hydrothermal biochar without fly ash is located at the lignin or carboxyl-containing fat area (Fig. 4f), which means the original hydrothermal biochar contains more aliphatic compounds. After the addition of fly ash, aliphatic compounds start converting to aromatic hydrocarbons (except H150-1:2), indicating that the addition of fly ash changes the chemical composition of hydrothermal biochar. The low aromaticity of H150-1:2, likely due to the lower preparation temperature, keeps it within the fat class region, highlighting the influence of preparation temperature on the stability of hydrothermal biochar.

Figure S4 is the corresponding XPS full spectrum of two biochar, the elemental percentages are listed in Table S3. The original hydrothermal biochar contains four elements, C, O, N and Si. However, the silicon content is minimal, suggesting that the amount of internal minerals in the biochar is negligible. The stability of the biochar is primarily influenced by the doping of fly ash. In comparison to the original hydrothermal biochar, the O content in the fly ash-doped hydrothermal biochar increased significantly, while the C content decreased. Elements such as Si, Al, Ca, Mg appeared after fly ash doping. With the rising of temperature, the content of O element decreases and the content of C increases, indicating that higher temperatures can enhance the carbon sequestration capacity.

The XPS fine spectrum of C, Si and Al enables a semi-quantitative analysis of biochar`s surface functional groups and provides insights into its stability. The fitting results are shown in Figs. 5, S5, and S6 and Table S4. In the C1s fine spectrum, the peak at 284.8 eV corresponds to C-H/C–C/C=C, while 286.6 eV indicates hydroxyl C–OH/C–O–C. The peak at 288.5 eV is attributed to carbonyl C=O and carboxyl O=C-O, and the peak at 289.5eV represents ester-COOR. 293.3eV is the peak of the halogenated hydrocarbon C-F3, and 296.1eV is considered to be the peak of the heteroatomic carbon bond C-X (Wanga et al. 2021). The peak at about 103 eV in the Si2p fine spectrum corresponds to the fitting peaks of Si2p1 and Si2p3 of SiO2. In the Al2p fine spectrum, the

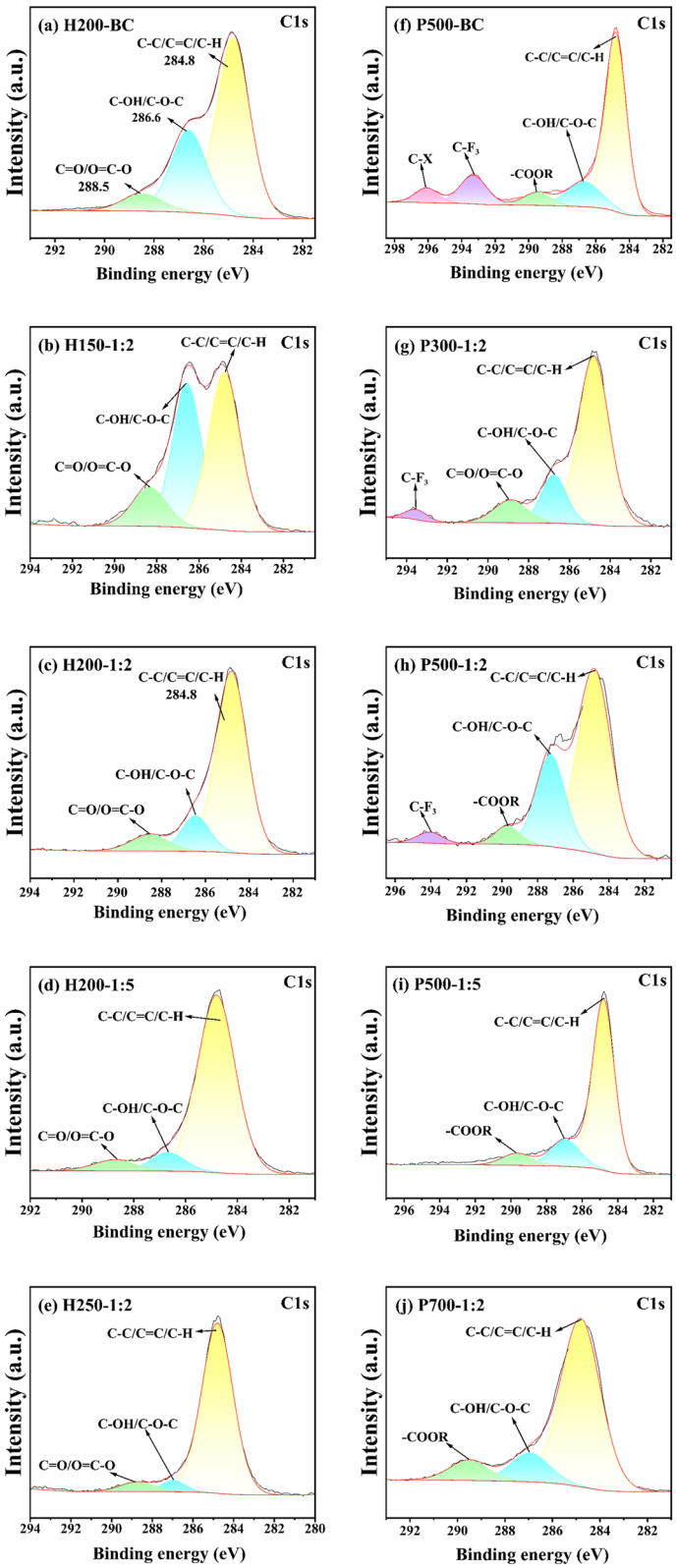

Fig. 5 C1s in XPS peak fitting of hydrothermal biochar (**a**, **b**, **c**, **d**, **e**) and pyrolysis biochar (**f**, **g**, **h**, **i**, **j**)

fitting peaks for Al2p1 and Al2p3 in Al2O3 are observed in the range of 73.5 to 75.5 eV.

The C1s fine spectrum of hydrothermal biochar reveals three characteristic peaks: C–C/C=C/C-H at 284 eV, hydroxyl C–OH/C–O–C at 286.6 eV, and carbonyl C=O/carboxyl O=C–C at 288.5 eV. Except for H150-1:2, the addition of fly ash leads to a decrease in oxygen-containing functional groups (C–OH and C–O–C) and an increase in C−C/C=C/C-H bonds, indicating an enhanced degree of aromatization in the biochar. However, with higher amounts of fly ash, the proportion of oxygen-containing functional groups, such as hydroxyl C–OH/C–O–C and carbonyl C=O/carboxyl O=C–C, increases. This may be due to reactions between oxide components (e.g., SiO_2 and Al_2O_3) from the fly ash and carbon from the biochar at elevated temperatures, which results in the formation of more oxygen-containing functional groups. The decrease in the C–C/C=C/C-H ratio suggests that adding excessive fly ash does not significantly enhance the stability of the biochar. As the hydrothermal temperature rises, the ratio of C–C/C=C/C-H gradually increases, while the proportion of oxygen-containing functional groups (e.g., hydroxyl C–OH/C–O–C and carbonyl C=O/carboxyl O=C–C) decreases, indicating that higher temperatures promote the formation of aromatic carbon at the expense of aliphatic groups. The fine spectra of Si2p and Al2p show that temperature and the addition of fly ash do not significantly affect the peak intensities of SiO_2 and Al_2O_3, suggesting that the morphology of silicon and aluminum remains stable.

Similar to hydrothermal biochar (Fig. S4, Table S3), pyrolysis biochar primarily consists of C and O, with negligible amounts of Mg and Si. Compared with the original pyrolysis biochar, O content increased, C content decreased, and Al, Mg, Ca, and other elements appeared, presumably due to the doping of fly ash in biochar. Consistent with the hydrothermal method, temperature is significant to the pyrolysis of biochar. With the increase of pyrolysis temperature, the O content of biochar decreases and the C content increases, indicating that higher pyrolysis temperature is conducive to improving the carbon sequestration capacity of biochar.

As shown in Figs. S5 and S6, the fine spectrum of Si 2p and Al 2p indicates that the addition of fly ash significantly affects the peak strength of the functional groups of SiO_2 and Al_2O_3. The percentages of Si and Al increased from 2.35% and 0% in P500-BC to 12.25% and 6.74% in P500-1:2, respectively. Although the morphology of silicon and aluminum remains largely unchanged, as confirmed by the fine spectra, the XRD patterns revealed

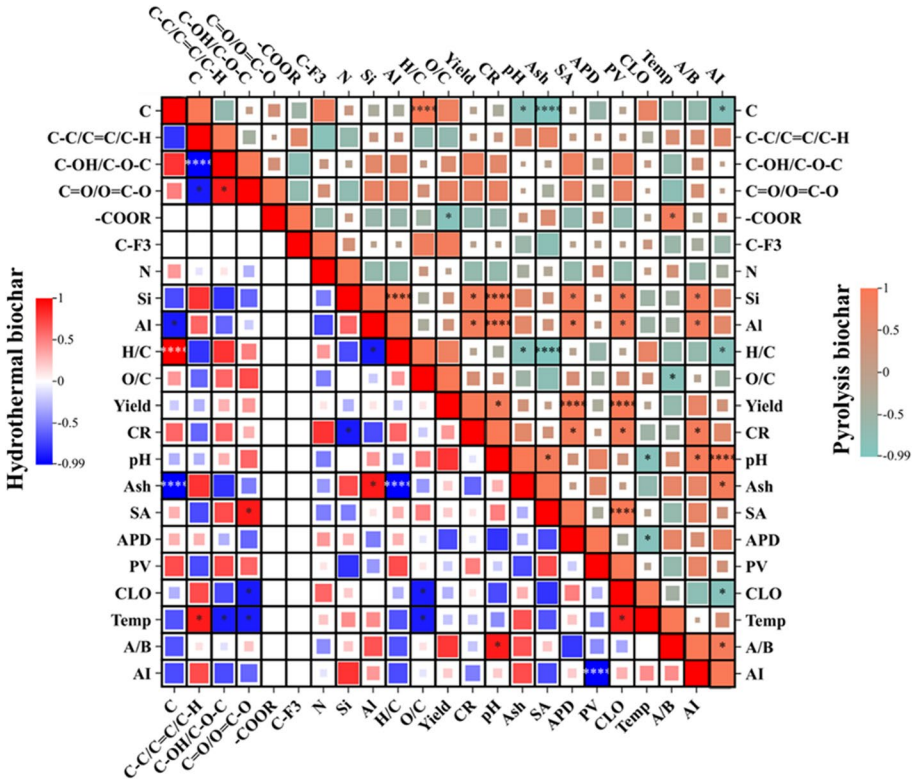

Fig. 6 Spearman correlation matrix of hydrothermal biochar and pyrolysis biochar

the presence of different crystalline silicon compounds in the various biochar samples (Fig. 4a). A variety of functional groups in P500-BC give rise to several distinctive peaks, such as C–C/C=C/C-H (284 eV), hydroxyl C–OH/ether bond C–O–C (286.6 eV), and carbonyl group C=O/O=C–C (288.5 eV), as shown by the fine spectra of C1s (Fig. 4). The peaks corresponding to ester-COOR (289.5 eV), halogenated hydrocarbon C-F3 (293.3 eV) and heteroatomic carbon bond C-X (296.1 eV) were also detected. Compared with BC, the proportion of oxygen-containing functional groups C–OH and C–O–C increased by 2.38%−13.78%. These findings suggest that the quantity of oxygen-containing functional groups on the surface rises with fly ash addition. Numerous studies have demonstrated that the addition of oxide-containing materials, such as clay, fatty acids, and iron oxide, can enhance the quantity of oxygen functional groups in biochar.

The C–C/C=C/C-H functional group ratio first increased and subsequently reduced along with the fly ash doping. The functional groups of biochar are impacted by the temperature during pyrolysis. The fraction of functional groups containing oxygen (i.e., hydroxyl C–OH/C–O–C and carbonyl C=O/carboxyl O=C–C) first rises and then drops with temperature, while C–C/C=C/C-H steadily increases (Table S4). This is presumably because fly ash injection plays a major part in lowering the temperature below 500 ℃. The abundant oxide components in fly ash contribute to strengthening the oxygen-containing functional groups within biochar. Above 500 °C, the pyrolysis temperature takes center stage, causing an increase in aromatic functional groups and a decrease in aliphatic functional groups like hydroxyl and carboxyl groups.

In summary, two production methods lead to different properties, energy consumption and carbon footprints of biochar. In our work, we focus on the characteristics that highly related with the effectiveness of soil carbon sequestration, such as stability and carbon retention (Gascó et al. 2018; Taskin et al. 2019; Luo et al. 2023). To assess the key factors influencing biochar utilization, we conducted a Spearman correlation coefficient (SCC) analysis between various properties of biochar (Xu et al. 2021). The values of carbon retention rate (CR) (Fig. 2) and carbon loss (CLO) by H_2O_2 oxidation (Fig. 4) were selected as the index to represent the potential for carbon sequestration and chemical-oxidation resistance, respectively. All basic properties of biochar were considered, including aromaticity (H/C ratio and AI, Table S1), average pore diameter, A/B ratio (fly ash/biomass), pore volume (i.e., APD, PV, Table S1), carbon functional groups from XPS analysis (Fig. 5), specific surface area (SSA, Table S1).

The SCC analysis (Fig. 6) showed no correlation between chemical stability and carbon retention rate in either hydrothermal or pyrolysis biochar ($p > 0.05$), indicating that different factors influence each type. In hydrothermal biochar, CR was negatively correlated with the Si element (−0.9, $p < 0.05$), which contrasted sharply with pyrolysis biochar. For pyrolysis biochar, CR showed positive correlations with the A/B ratio (0.89, $p < 0.05$), PV (0.9, $p < 0.05$), SA (0.9, $p < 0.05$), and both Si (1.0, $p < 0.01$) and Al (1.0, $p < 0.01$) elements, indicating a significant enhancement in CR due to the addition of fly ash. This suggests that fly ash modification is more beneficial for pyrolysis biochar than for hydrothermal biochar. The CLO of hydrothermal biochar was negatively associated with the C=O/O=C-O groups (−0.9, $p < 0.05$) and the O/C ratio (−0.9, $p < 0.05$), while positively correlated with synthesis temperature (0.89, $p < 0.05$). This implies that higher temperatures result in lower O content and increased carbon loss during H_2O_2 oxidation. Conversely, the CLO of pyrolysis biochar was negatively correlated with the AI (−0.9, $p < 0.05$), APD (−0.9, $p < 0.05$), and pH (−0.9, $p < 0.05$). A higher AI suggests a greater presence of stable aromatic carbon, which enhances chemical oxidation resistance. Furthermore, the AI was positively correlated with the A/B ratio, further confirming the advantages of fly ash addition.

4 Conclusion

In this study, fly ash was used as an additive to prepare biochar materials by hydrothermal and pyrolysis methods. The effects of the preparation process and fly ash adding ratio were investigated by analyzing the physicochemical properties, microstructure characterization, and stability of biochar. The findings demonstrated that adding fly ash and raising the preparation temperature could improve the thermal and chemical stability of pyrolysis biochar. This is because the addition of fly ash and the raised preparation temperature encouraged the production of aromatic carbon as well as the breakdown and transformation of aliphatic carbon in biochar, thereby enhancing the stability of the material. Fly ash doping improves the specific surface area and pore volume of biochar by promoting the formation of micropores and enlarging them into mesopores. According to SEM–EDS, XRD, and FTIR characterization, pyrolysis biochar contains crystalline quartz (SiO_2), mullite ($3Al_2O_3{\cdot}2SiO_2$), and T-O/T-O-T stretching vibration (T: Si/Al), indicating that fly ash is successfully loaded on biochar. Furthermore, SiO_2 and Al_2O_3 reacted with NaOH to produce albite, sodium silicaluminate, and other minerals that adhere to the surface of the material and shield it from oxidation. In contrast, while fly ash was successfully incorporated,

hydrothermal biochar did not show similar benefits in terms of carbon retention and chemical stability. Overall, it is assumed that fly ash-doped pyrolysis biochar offers enormous promise for soil carbon sequestration, and that fly ash as a mineral additive can enhance the ability of biochar to sequester carbon during pyrolysis. Future research should focus on the energy consumption and carbon footprints of soil carbon sequestration induced by fly ash-doped biochar from its feedstock preparation to production and final application, including the assessment of the cost and efficiency. The fly ash-doped biochar using in carbon sequestration is a promising negative emission technology that requires more investigation.

Supplementary Information

The online version contains supplementary material available at https://doi.org/10.1007/s44246-024-00185-2.

Supplementary Material 1

Acknowledgements
We acknowledge the School of Chemical and Environmental Engineering, China University of Mining and Technology, Beijing, China for providing the required support that ensured the completion of the research.

Authors' contributions
All authors contributed to the study conception and design. Material preparation, data collection and analysis were performed by Gang Li, Shumin Wu, Wei Chen and Yan Ma. The first draft of the manuscript was written by Rongchuan Ye and all authors commented on previous versions of the manuscript. All authors read and approved the final manuscript.

Funding
This work was supported by Natural Science Foundation of Beijing Municipality, General Program [Grant No. 8222072], the Key Laboratory of Agro-Environment in Downstream of Yangze Plain, Ministry of Agriculture and Rural Affairs [Grant No. 2023F03], State Key Laboratory of Mineral Processing, 2023.01–2024.12 Open Foundation of State Key Laboratory of Mineral Processing [Grant No. BGRIMM-KJSKL-2023–24], Highway traffic environmental protection technology transportation industry key laboratory open project. State Key Laboratory of Coal Resources and Safe Mining, Open Fund Project [Grant No. SKLCRSM22KFA14].

Data availability
All data associated with this study can be found within the main manuscript and the Supplementary Material, and sources are stated.

Declarations

Competing interests
The authors declare that they have no known competing financial interests or personal relationships that could have influenced the work reported in this paper.

Author details
[1]Department of Ecology and Environment of Xinjiang Uygur Autonomous Region, Urumqi 830000, China. [2]Key Laboratory of Agro-Environment in Downstream of Yangze Plain, Ministry of Agriculture and Rural Affairs, P. R. China, Nanjing 210000, China. [3]School of Chemical and Environmental Engineering, China University of Mining and Technology, Beijing 100083, China. [4]China Energy LongYuan Environmental Protection Co., Ltd, Beijing 100039, China. [5]Beijing Building Materials Academy of Sciences Research Co.,Ltd: Beijing Building Materials Testing Academy Co., Ltd, Beijing 100041, China.

Received: 22 July 2024 Revised: 15 December 2024 Accepted: 16 December 2024
Published online: 06 February 2025

References

Ahmad M, Ahmad M, Usman ARA et al (2019) Date palm waste-derived biochar composites with silica and zeolite: synthesis, characterization and implication for carbon stability and recalcitrant potential. Environ Geochem Health 41:1687–1704. https://doi.org/10.1007/s10653-017-9947-0
Akanksha B, Shilpa N, Khadim H et al (2022) Effect of temperature and fly ash content on the catalytically pyrolyzed rice straw biochar–fly ash composites for methylene blue adsorption. Asia-Pac J Chem Eng 17:e2828. https://doi.org/10.1002/apj.2828
Aktar S, Hossain MA, Rathnayake N et al (2022) Effects of temperature and carrier gas on physico-chemical properties of biochar derived from biosolids. J Anal Appl Pyrol 164:105542. https://doi.org/10.1016/j.jaap.2022.105542
Awad YM, Ok YS, Abrigata J et al (2018) Pine sawdust biomass and biochars at different pyrolysis temperatures change soil redox processes. Sci Total Environ 625:147–154. https://doi.org/10.1016/j.scitotenv.2017.12.194
Babin A, Vaneeckhaute C, Iliuta MC (2021) Potential and challenges of bioenergy with carbon capture and storage as a carbon-negative energy source: a review. Biomass Bioenerg 146:105968. https://doi.org/10.1016/j.biombioe.2021.105968
Bhardwaj A, Nag S, Hussain K et al (2022) Effect of temperature and fly ash content on the catalytically pyrolyzed rice straw biochar-fly ash composites for methylene blue adsorption. Asia-Pac J Chem Eng 17:2828. https://doi.org/10.1002/apj.2828
Chen B, Zhou D, Zhu L (2008) Transitional adsorption and partition of nonpolar and polar aromatic contaminants by biochars of pine needles with different pyrolytic temperatures. Environ Sci Technol 42:5137–5143. https://doi.org/10.1021/es8002684
Chen Y, Zwieten VL, Xiao K et al (2024) Biochar as a green solution to drive the soil carbon pump. Carbon Res 3:44. https://doi.org/10.1007/s44246-024-00132-1
Deng X, Teng F, Chen M et al (2024) Exploring negative emission potential of biochar to achieve carbon neutrality goal in China. Nat Commun 15:1085. https://doi.org/10.1038/s41467-024-45314-y
Dumanlı GA, Windle HA (2012) Carbon fibres from cellulosic precursors: a review. J Mater Sci 47:4236–4250. https://doi.org/10.1007/s10853-011-6081-8
Fan X, Wang X, Zhao B et al (2022) Sorption mechanisms of diethyl phthalate by nutshell biochar derived at different pyrolysis temperature. J Environ Chem Eng 10:107328. https://doi.org/10.1016/jece.2022.107328
Fu M, Mo C, Li H et al (2019) Comparison of physicochemical properties of biochars and hydrochars produced from food wastes. J Clean Prod 236:117637. https://doi.org/10.1016/j.jclepro.2019.117637
Gascó G, Paz-Ferreiro J, Álvarez ML et al (2018) Biochars and hydrochars prepared by pyrolysis and hydrothermal carbonization of pig manure. Waste Manage 79:395–403. https://doi.org/10.1016/j.wasman.2018.08.015
Han L, Ro KS, Wang Y et al (2018) Oxidation resistance of biochars as a function of feedstock and pyrolysis condition. Sci Total Environ 616:335–344. https://doi.org/10.1016/j.scitotenv.2017.11.014
Johannes L, Stephen J (2012) Biochar for environmental management: science and technology. Taylor and Francis. 976. https://doi.org/10.4324/9781849770552
Kan Z, Liu Q, Wu G et al (2020) Temperature and moisture driven changes in soil carbon sequestration and mineralization under biochar addition. J Clean Prod 265:121921. https://doi.org/10.1016/j.jclepro.2020.121921
Lane J, Greig C, Garnett A (2021) Uncertain storage prospects create a conundrum for carbon capture and storage ambitions. Nat Clim Change 11:925–936. https://doi.org/10.1038/s41558-021-01175-7
Leng L, Huang H (2018) An overview of the effect of pyrolysis process parameters on biochar stability. Bioresource Technol 270:627–642. https://doi.org/10.1016/j.biortech.2018.09.030

Li F, Cao X, Zhao L et al (2014) Effects of mineral additives on biochar formation: carbon retention, stability, and properties. Environ Sci Technol 48(19):11211–11217. https://doi.org/10.1021/es501885n
Li N, Qiao X, Liu Y et al (2015) Oxidization of dissolved organic matters from different sources by hydroxyl radical. J Environ Chem 34(7):1246–1251. https://doi.org/10.7524/j.issn.0254-6108.2015.07.2014121707
Liu G, Pan X, Ma X et al (2020a) Effects of feedstock and inherent mineral components on oxidation resistance of biochars. Sci Total Environ 726:138672. https://doi.org/10.1016/j.scitotenv.2020.138672
Liu Y, Gao C, Wang Y et al (2020b) Vermiculite modification increases carbon retention and stability of rice straw biochar at different carbonization temperatures. J Clean Prod 254:120111. https://doi.org/10.1016/j.jclepro.2020.120111
Liu H, Xu G, Li G (2021) Preparation of porous biochar based on pharmaceutical sludge activated by NaOH and its application in the adsorption of tetracycline. J Colloid Interf Sci 587:271–278. https://doi.org/10.1016/j.jcis.2020.12.014
Lu J, Yang YQ, Liu PX et al (2020) Iron-montmorillonite treated corn straw biochar: interfacial chemical behavior and stability. Sci Total Environ 708:134773. https://doi.org/10.1016/j.scitotenv.2019.134773
Luo L, Wang J, Lv J et al (2023) Carbon sequestration strategies in soil using biochar: advances, challenges, and opportunities. Environ Sci Technol 57:11357–11372. https://doi.org/10.1021/acs.est.3c02620
Ma Y, Shang X, Zhang Y et al (2024) Co-pyrolysis of alkali-fused fly ash and corn stover to synthesize biochar composites for remediating lead-contaminated soil. Environ Res 252:118938. https://doi.org/10.1016/j.envres.2024.118938
Majumder S, Neogi S, Dutta T et al (2019) The impact of biochar on soil carbon sequestration: meta-analytical approach to evaluating environmental and economic advantages. J Environ Manage 250:109466.1–109466.11. https://doi.org/10.1016/j.jenvman.2019.109466
Nan H, Yang F, Zhao L et al (2019) Interaction of inherent minerals with carbon during biomass pyrolysis weakens biochar carbon sequestration potential. Acs Sustainable Chem Eng 7:1591–1599. https://doi.org/10.1021/j.acssuschemeng.2019.8b05364
Oleszczuk P, Ćwikła-Bundyra W, Bogusz A et al (2016) Characterization of nanoparticles of biochars from different biomass. J Anal Appl Pyrol 121:165–172. https://doi.org/10.1016/j.jaap.2016.07.017
Patwardhan PR, Satrio JA, Brown RC et al (2010) Influence of inorganic salts on the primary pyrolysis products of cellulose. Bioresource Technol 101:4646–4655. https://doi.org/10.1016/j.biortech.2010.01.112
Pereira RC, Kaal J, Arbestain MC (2011) Contribution to characterization of biochar to estimate the labile fraction of carbon. Org Geochem 42:1331–1342. https://doi.org/10.1016/j.orggeochem.2011.09.002
Rawal A, Joseph SD, Hook JM et al (2016) Mineral-biochar composites: molecular structure and porosity. Environ Sci Technol 50:7706–7714. https://doi.org/10.1021/acs.est.6b00685
Ren N, Tang Y, Li M (2018) Mineral additive enhanced carbon retention and stabilization in sewage sludge-derived biochar. Process Saf Environ 115:70–78. https://doi.org/10.1016/j.psep.2017.11.006
Sahoo PK, Tripathy S, Panigrahi MK et al (2013) Evaluation of the use of an alkali modified fly ash as a potential adsorbent for the removal of metals from acid mine drainage. Appl Water Sci 3:567–576. https://doi.org/10.1007/s13201-013-0113-2
Shin J, Park D, Hong S et al (2021) Influence of activated biochar pellet fertilizer application on greenhouse gas emissions and carbon sequestration in rice (Oryza sativa L.) production. Environ Pollut 285:117457. https://doi.org/10.1016/j.envpol.2021.117457
Sun Z, Zhang Z, Zhu K et al (2020) Biochar altered native soil organic carbon by changing soil aggregate size distribution and native SOC in aggregates based on an 8-year field experiment. Sci Total Environ 708:134829. https://doi.org/10.1016/j.scitotenv.2019.134829
Taskin E, Bueno CC, Allegretta I et al (2019) Multianalytical characterization of biochar and hydrochar produced from waste biomasses for environmental and agricultural applications. Chemosphere 233:422–430. https://doi.org/10.1016/j.chemosphere.2019.05.204
Tomczyk A, Sokolowska Z, Boguta P (2020) Biochar physicochemical properties: pyrolysis temperature and feedstock kind effects. Rev Environ Sci Biotechnol 19:191–215. https://doi.org/10.1007/s11157-020-09523-3
Wang Y, Yin R, Liu R (2014) Characterization of biochar from fast pyrolysis and its effect on chemical properties of the tea garden soil. J Anal Appl Pyrolysis 110:375–381. https://doi.org/10.1016/j.jaap.2014.10.006
Wang X, Chi Q, Liu X et al (2019) Influence of pyrolysis temperature on characteristics and environmental risk of heavy metals in pyrolyzed biochar made from hydrothermally treated sewage sludge. Chemosphere 216:698–706. https://doi.org/10.1016/j.chemosphere.2018.10.189
Wang K, Peng N, Sun J et al (2020a) Synthesis of silica-composited biochars from alkali-fused fly ash and agricultural wastes for enhanced adsorption of methylene blue. Sci Total Environ 729:139055. https://doi.org/10.1016/j.scitotenv.2020.139055
Wang H, Xu J, Sheng L (2020b) Preparation of straw biochar and application of constructed wetland in China: a review. J Clean Prod 273:123131. https://doi.org/10.1016/j.jclepro.2020.123131
Wang F, Jin L, Guo C et al (2021a) Enhanced heavy metals sorption by modified biochars derived from pig manure. Sci Total Environ 786:147595. https://doi.org/10.1016/j.scitotenv.2021.147595
Wang K, Peng N, Niu X, et al (2021b) Effects of aging on surface properties and endogenous copper and zinc leachability of swine manure biochar and its composite with alkali-fused fly ash. Waste Manage 126. https://doi.org/10.1016/j.wasman.2021.03.042
Wang H, Wang X, Teng H et al (2022a) Purification mechanism of city tail water by constructed wetland substrate with NaOH-modified corn straw biochar. Ecotox Environ Safe 238:113597. https://doi.org/10.1016/j.ecoenv.2022.113597
Wang F, Zhang RL, Donne SW et al (2022b) Co-pyrolysis of wood chips and bentonite/kaolin: influence of temperatures and minerals on characteristics and carbon sequestration potential of biochar. Sci Total Environ 838:156081. https://doi.org/10.1016/j.scitotenv.2022.156081
Wang M, Zhang M, Chen X et al (2022c) Hydrothermal conversion of Chinese cabbage residue for sustainable agriculture: influence of process parameters on hydrochar and hydrolysate. Sci Total Environ 812:152478. https://doi.org/10.1016/J.SCITOTENV.2021.152478
Wang L, Deng J, Yang X et al (2023) Role of biochar toward carbon neutrality. Carbon Res 2:2. https://doi.org/10.1007/s44246-023-00035-7
Wanga K, Penga N, Niu X et al (2021) Effects of aging on surface properties and endogenous copper and zinc leachability of swine manure biochar and its composite with alkali-fused fly ash. Waste Manag 126:400–410. https://doi.org/10.1016/j.wasman.2021.03.042
Werner R, Yao D (1992) Rate constants for reaction of hydroxyl radicals several drinking water contaminants. Environ Sci Technol 26:1005–1013. https://doi.org/10.1021/es00029a021
Williams PT, Horne PA (1994) The role of metal salts in the pyrolysis of biomass. Renew Energ 4:1–13. https://doi.org/10.1016/j.ret.1994.0960-1481
Wu J, Wang T, Li S et al (2024) A green method to improve adsorption capacity of hydrochar by ball-milling: enhanced norfloxacin adsorption performance and mechanistic insight. Carbon Research 3:60. https://doi.org/10.1007/s44246-024-00145-w
Xiao X, Chen Z, Chen B (2016) H/C atomic ratio as a smart linkage between pyrolytic temperatures, aromatic clusters and sorption properties of biochars derived from diverse precursory materials. Sci Rep 6:22644. https://doi.org/10.1038/srep22644
Xiao R, Wang J, Gaston L et al (2018) Biochar produced from mineral salt-impregnated chicken manure: fertility properties and potential for carbon sequestration. Waste Manag 78:802–810. https://doi.org/10.1016/j.wasman.2018.06.047
Xu Z, He M, Xu X et al (2021) Impacts of different activation processes on the carbon stability of biochar for oxidation resistance. Bioresour 338:125555. https://doi.org/10.1016/j.biortech.2021.125555
Yang F, Zhao L, Gao B et al (2016) The interfacial behavior between biochar and soil minerals and its effect on biochar stability. Environ Sci Technol 50:2264–2271. https://doi.org/10.1021/j.acs.est.2016.5b03656
Yang Y, Sun K, Han L et al (2018) Effect of mineralson the stability of biochar. Chemosphere 204:310–317. https://doi.org/10.1016/j.chemosphere.2018.04.057
Yang W, Lei G, Quan S et al (2022) The removal of Cr (VI) from aqueous solutions with corn stalk biochar. Int J Env Res Pub He 19:14188. https://doi.org/10.3390/ijerph192114188
Yun X, Ma Y, Zheng H et al (2022) Pb (II) adsorption by biochar from co-pyrolysis of corn stalks and alkali-fused fly ash. Biochar 4:66. https://doi.org/10.1007/S42773-022-00189-4

Zhao Z, Nie T, Zhou W (2019) Enhanced biochar stabilities and adsorption properties for tetracycline by synthesizing silica-composited biochar. Environ Pollut 254:113015. https://doi.org/10.1016/j.envpol.2019.113015
Zhou Z, Li Z, Zhang Z et al (2021) Treatment of the saline-alkali soil with acidic corn stalk biochar and its effect on the sorghum yield in western Songnen Plain. Sci Total Environ 797:149190. https://doi.org/10.1016/j.scitotenv.2021.14190
Zong Y, Xiao Q, Lu S (2020) Biochar derived from cadmium-contaminated rice straw at various pyrolysis temperatures: cadmium immobilization mechanisms and environmental implication. Bioresource Technol 321:124459. https://doi.org/10.1016/j.biortech.2020.124459

Publisher's Note